Hindawi
Geofluids
Volume 2019, Article ID 9797326, 15 pages
https://doi.org/10.1155/2019/9797326

Research Article

Linear Correlation of Ba and Eu Contents by Hydrothermal Activities: A Case Study in the Hetang Formation, South China

Chao Chang,[1,2] **Qi Fu**,[3] **and Xiaolin Wang**[2]

[1]*Shaanxi Key Laboratory of Early Life and Environment, State Key Laboratory of Continental Dynamics, and Department of Geology, Northwest University, Xi'an 710069, China*
[2]*State Key Laboratory for Mineral Deposits Research, Institute of Energy Sciences, School of Earth Sciences and Engineering, Nanjing University, Nanjing 210046, China*
[3]*Department of Earth and Atmospheric Sciences, University of Houston, Houston, TX 77204, USA*

Correspondence should be addressed to Chao Chang; changchao@nwu.edu.cn

Received 28 November 2018; Accepted 11 February 2019; Published 1 April 2019

Academic Editor: Stefano Lo Russo

A significant linear correlation between Ba and Eu contents has been observed in a set of mudrock formations in the lower Cambrian Hetang Formation in South China. Combined with petrographic features and reinvestigation of published data obtained from the same laboratory, the analytical interference of Ba can be excluded as a main factor of this correlation. Electron microprobe analyses (EMPA) have indicated that Ba-rich minerals (hyalophane and cymrite) precipitated from hydrothermal fluids account for the total Ba content. It is evident that significant contribution of both Ba and Eu from hydrothermal fluids is the cause of this linear relationship, while this coexistence is ultimately controlled by their similar chemical properties and abundances in rock sequences along the fluid path. This interpretation was supported by similar linear Ba-Eu correlations retrieved from barite-bearing chert in another area of the Yangtze platform during the same geological period. Therefore, linear Ba-Eu correlations may be more common than previously thought in this area, where hydrothermal activities were active during the specific time interval.

1. Introduction

The rare earth elements (REEs) include lanthanum (La) and the f-block elements (cerium through lutetium) in the periodic table, whose atomic number ranges from 57 to 71. Scandium and yttrium are also included in this group as they have ionic radii similar to the lighter f-block elements and are found coexisting in the same ores (Atwood, 2012). The REEs are insoluble in most geological settings and resistant to remobilization beyond the mineralogical scale during weathering, diagenetic, and metamorphic processes. That makes them important tracers for characterizing and understanding a variety of geochemical "reservoirs" ([1, 2]; Atwood, 2012).

The most stable oxidation state of all REEs is the REE (III) form, except for europium (Eu) and cerium (Ce) that are also present in the form of Eu^{2+} and Ce^{4+}, respectively [3]. The distinctive redox chemistries of Eu and Ce are of considerable importance to understanding geochemical conditions with unique insights into magmatic, aqueous, and sedimentary processes ([1, 2, 4–6]; Murray et al., 1990; Atwood, 2012). The ionic radius of Eu^{2+} is about 17% larger than that of Eu^{3+}, which leads to different substitution behaviors of Eu^{2+} than other trivalent REEs (e.g., Sm and Gd) and subsequent anomalous REE patterns (i.e., Eu anomalies). Europium occurs in the form of Eu^{2+} under highly reducing conditions. It exists only within certain magmatic and/or hydrothermal environments that are rarely found at the surface of the Earth. An important geological example is that Eu can be highly concentrated in plagioclase feldspar by substituting into the calcium site. The anomalous Eu abundance in magmatic rocks indicates relatively shallow igneous partial melting or fractional crystallization processes (Atwood, 2012). Positive Eu anomalies have also been widely reported in modern deep-sea hydrothermal systems [7–9] and in massive deposits of submarine hydrothermal exhalative origin [10–12]. Consequently, it has been used as an

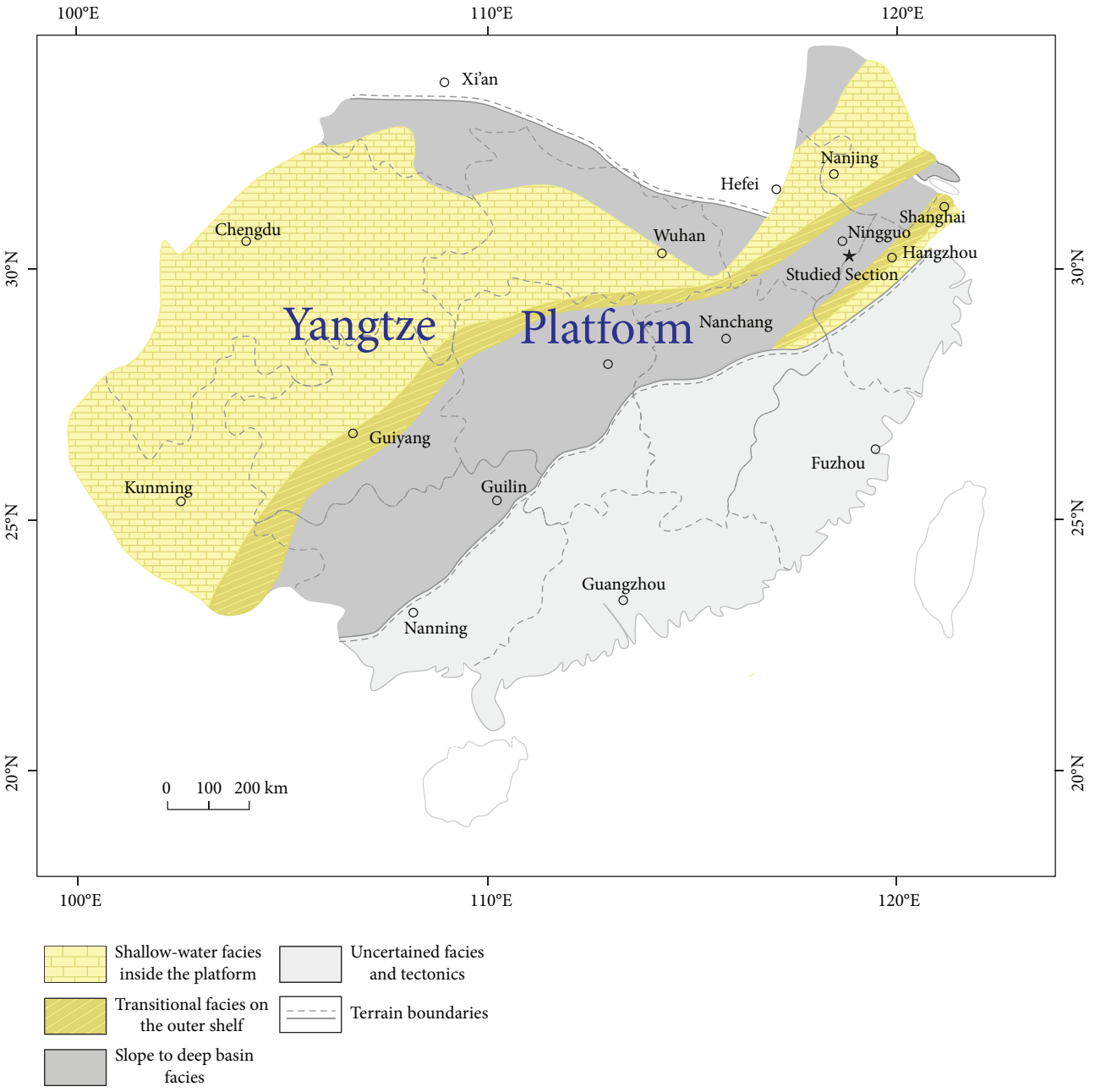

Figure 1: Simplified paleogeographic map of the Yangtze platform during the Cambrian (after [20]).

effective tracer for tracking and characterizing hydrothermal activities in sedimentary rocks and ore deposits [13–19]. In addition, in spite of no direct evidence showing europium reduction under surface conditions, positive Eu anomalies might be present at highly reducing conditions during diagenesis. For example, the trace and rare earth element abundances in phosphate nodules from the lower Cambrian strata in South China have shown positive Eu anomalies, possibly implying the replacement of Ca^{2+} by Eu^{2+} under reducing conditions [20].

Accurate measurement of Eu abundances in geological samples is a prerequisite to effectively obtaining important information of geochemical reactions and environmental conditions in natural processes recorded by elements. The determination of Eu abundances by inductively coupled plasma-mass spectrometry (ICP-MS), however, is interfered by the coexisting element of barium (Ba). This is due to similar mass/charge ratios of Ba oxide (BaO) and hydroxide ($BaOH^+$) species that partially overlap those of Eu isotopes (^{151}Eu and ^{153}Eu), with ^{151}Eu being less affected by BaO and $BaOH^+$ than ^{153}Eu [21–23].

A routine assessment of the interference level of Ba is to determine the yield of Ba oxide and hydroxide species using a single-element solution of Ba (e.g., 500 ng/ml Ba in $BaCl_2$ solution) and compare the yield of potential interfering species (e.g., $^{135}Ba^{16}O$) with the Eu isotope that has the same

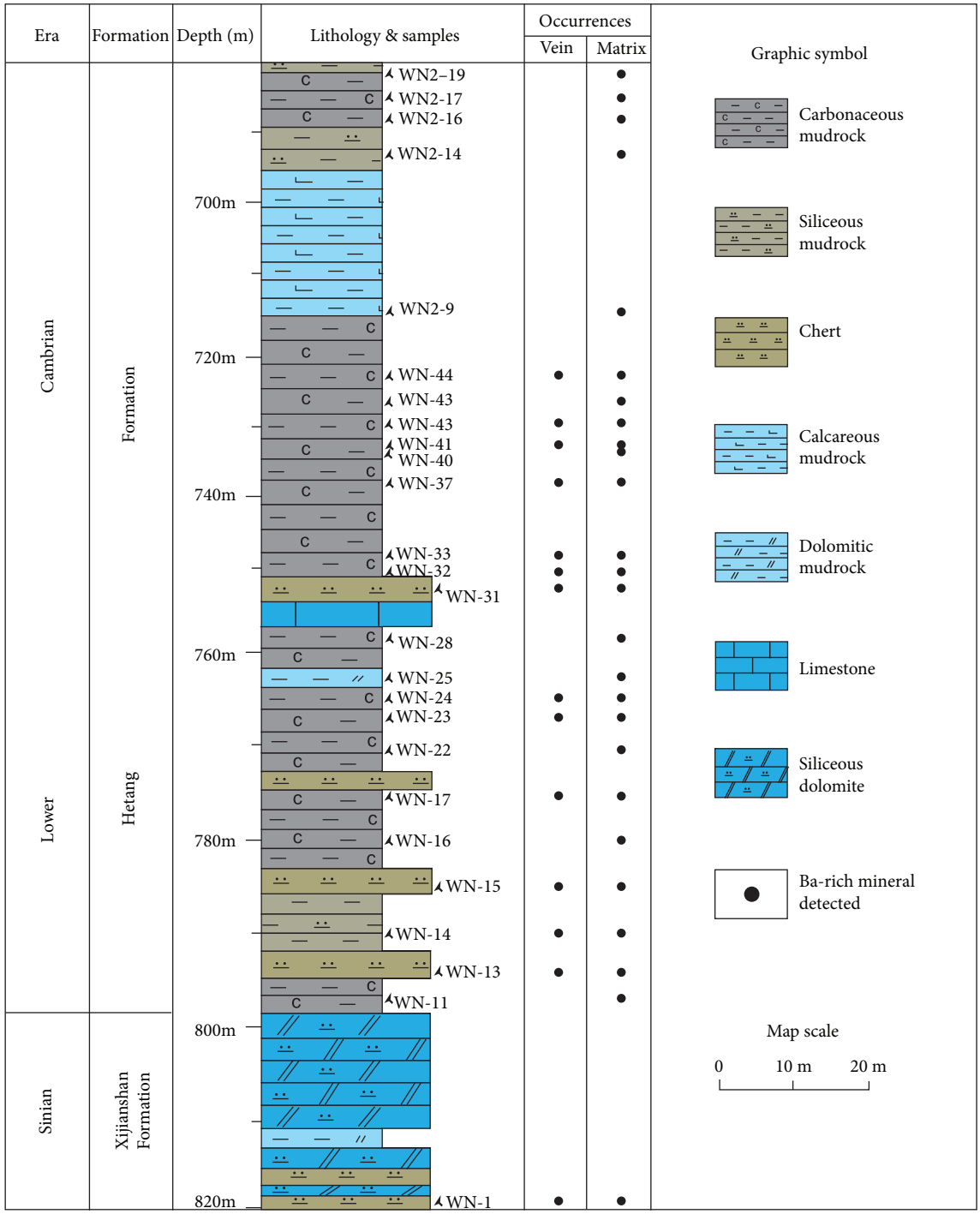

Figure 2: Petrological profile of Well Wanning 2. The depth of each sample analyzed by EMPA is labelled, along with the occurrence of Ba-rich minerals.

mass number (e.g., ^{151}Eu) in a single-element solution of Eu [21, 24]. The previous results indicated that 1000 ng/g of Ba could cause an apparent Eu concentration of 0.22 ng/g in ^{151}Eu [21]. An alternative way to evaluate the extent of the interference is analyzing the correlation between Ba and Eu in the samples. Plots of Ba and Eu have been widely used in previous studies, and linear Ba-Eu correlation has been commonly interpreted as an indicator of apparent interference of Ba with Eu, with less attention on other possible causes ([5, 20, 25]; Ling et al., 2013).

To better understand the ultimate controlling factors, if any, of Ba-Eu correlation other than analytical errors embedded with analytical techniques, we investigated the trace and rare earth elemental contents of a drilling profile in the lower

Cambrian Hetang Formation, South China. Hydrothermal activities and Ba enrichment have been reported in previous studies for this formation and its stratigraphic equivalents in other areas [16, 25–28]. In this study, a series of petrological and mineralogical analytical techniques are used to quantify the abundances of Eu and Ba and elucidate their relationship with hydrothermal activities.

2. Geological Setting and Samples

During the transition between the Ediacaran period and the Cambrian period, the Yangtze platform in South China gradually evolved from a rift to a passive continental margin basin in response to extensional tectonism [29, 30]. With sedimentological features, the sedimentary sequences can be classified into three distinct facies: shallow water, transitional, and slope to deep basin facies (Figure 1). The shallow water facies is represented by thick carbonate strata, while the slope to deep basin facies consists of a series of interbedded black chert and shale. The transitional facies is composed of both carbonate and black shale [20, 29]. The occurrence of ore deposit beds containing Ni-Mo-PGE-Au sulfides has been reported in this black shale-chert sequence along the NE transitional belt at the margins of the Yangtze platform in lower Cambrian [15].

The samples in this study were taken from a drilling section (Well Wanning 2) located at Ningguo, Anhui province (Figure 1), covering lithological units of the Xijianshan and Hetang formations. The sedimentary strata of the Hetang Formation include mudrock, chert, and carbonates. The major mineralogy of mudrock varies, including carbonaceous materials, silicates, or Ca-containing minerals. The Hetang Formation is underlain by the Xijianshan Formation which is mainly composed of dolostone and chert. Carbonate and quartz veins are common in this set of strata, indicating enhanced fluid migration during diagenesis. The samples cover the whole depth of the Hetang Formation and are extended into the Xijianshan Formation (Figure 2). To ensure accurate measurements, two batches of samples with similar mineralogy and petrographic features at selected depths were collected for analyses (see below).

3. Methods

The trace element analysis was carried out on a Finnigan Element II ICP-MS at the State Key Laboratory for Mineral Deposits Research at Nanjing University. For carbonate rocks, 100 mg of powdered samples was weighted in Teflon beakers and dissolved by 1 M HAc under ultrasonic bathing for 2 hours. For mudrock and chert, 50 mg of powdered sample was dissolved by a mixed HF-HNO_3 solution in high-pressure Teflon bombs. For calcareous or dolomitic mudrock, the carbonate fractions were dissolved by 1 M HAc and the solid residues were then dissolved by the same mixed acid solution in high-pressure Teflon bombs. After dissolution, the solutions were centrifuged and the supernatants were transferred to clean Teflon beakers for evaporation. The solutions were added with 1 ml of HNO_3 and dried three times to remove HAc or HF. The residues were then dissolved in 5% HNO_3 solution for analysis. A solution containing Rh in 10 ppb was used as an internal standard to monitor signal drifting during measurements. The detailed analytical procedure was described in the work of Gao et al. [31], and parameters for the instrument were presented in Table 1. Analytical uncertainties are estimated to be less than 10%. The value of Eu/Eu^* is calculated as $2Eu_{PAAS}/(Sm_{PAAS} + Gd_{PAAS})$, where Eu_{PAAS}, Sm_{PAAS}, and Gd_{PAAS} represent the abundances of Eu, Sm, and Gd, respectively, normalized by the post-Archean Australian Shale (PAAS) standard [32].

Table 1: Parameters of the instrument.

Forward power	1200 W
Reflected power	2 W
Plasma gas flow rate	14.5 l/min
Auxiliary gas flow rate	0.8 l/min
Nebulizer gas flow rate	0.85 l/min
Sample uptake rate	1 ml/min
Resolution	300
Points per mass	15
Integration time	0.01 s/point
Sweeps	3

The electron microprobe analysis (EMPA) was carried out on polished, carbon-coated thin sections to study the petrological and mineralogical features in the samples. It was conducted using a JEOL JXA-8100 electron microprobe with a wavelength-dispersive system at the State Key Laboratory for Mineral Deposits Research at Nanjing University. The instrument was operated with three crystal spectrometers, with the accelerating voltage and the specimen current of 15 kV and 20 mA, respectively. The diameter of the beam spot used for quantitative element analysis was 1 μm. The standards used were natural minerals supplied by the American National Standards Institute (ANSI). The detection limit of the microprobe analysis was approximately 0.002% for each element.

4. Results

4.1. Petrological and Mineralogical Features. The locations of samples analyzed by EMPA within the profile are labelled in Figure 2. Minerals containing Ba and K, such as hyalophane and cymrite, were found in all of the mudrock and chert samples with backscattered electron (BSE) observation and EMPA analyses. For each sample analyzed by EMPA, the occurrence of Ba-rich minerals, in hydrothermal veins and/or in matrix, is also specified (Figure 2).

Hyalophane is present as the matrix in all the samples analyzed, while hydrothermal veins that contain hyalophane are observed in most samples. In matrices, the occurrence of hyalophane includes fillings of pore spaces in chert samples (Figure 3(a)) and thin rims around clastic K-feldspar grains (Figures 3(b)–3(d)). In hydrothermal veins, hyalophane is present as irregular or amorphous aggregates. The close

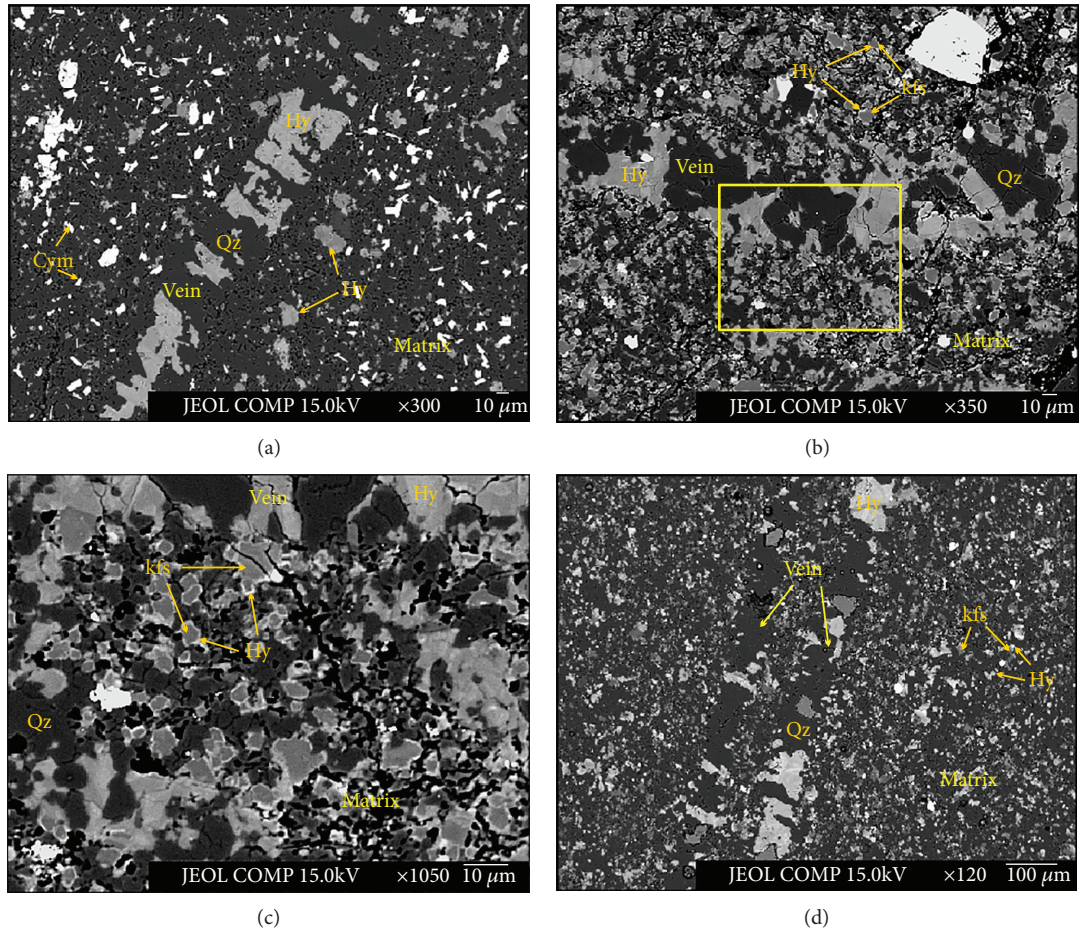

Figure 3: The occurrences of Ba-rich minerals. (a) Hyalophane grains in the vein matrix and a hydrothermal vein and cymrite in the matrix, sample WN-13. Both hyalophane and cymrite in the matrix occur as fillings of interparticle pores. Note that some hyalophane aggregates in veins are connected to those in the matrix. (b) Hyalophane in veins and in the matrix, sample WN-19. Nearly all the clastic K-feldspar grains are surrounded by hyalophane rims. Some hyalophane aggregates in veins are connected to hyalophane rims in the matrix. (c) Closeup of the marked area in (b), sample WN-19. Hyalophane rims can be easily distinguished from clastic K-feldspar cores by the difference in brightness. Hyalophane in veins and in the matrix is closely associated. (d) Hyalophane in veins and the matrix, sample WN-44. Hy: hyalophane; Cym: cymrite; Qz: quartz.

association of hyalophane in veins with the whole matrix is very common (Figure 3). In particular, the texture of hyalophane-bearing veins penetrating into the matrix is observed, with abundant hyalophane rims formed around clastic K-feldspar grains (Figures 3(b) and 3(c)). Cymrite grains show euhedral tabular forms, primarily coexisting with hyalophane in the matrix in a number of chert samples (Figure 3(a)).

4.2. Trace and Rare Earth Elements. Samples over the whole profile, Batch 1, were measured by ICP-MS for abundances of trace and rare earth elements, including carbonates, mudrock, and chert (Table 2). To limit analytical errors from instruments, a second batch of samples, i.e., Batch 2, with similar mineral compositions and petrological features were also used for analyses (Table 3).

There are 7 carbonate samples in Batch 1, including dolostone and limestone. The concentration of Ba and Eu in carbonates ranges from 76.67 to 326.92 ppm (Figure 4(a)) and 0.19 to 0.45 ppm (Figure 4(b)), respectively. Slight negative Eu anomalies are observed, with Eu/Eu^* values from 0.71 to 0.99 (Figure 4(c)). There is a covariation of Sm and Gd concentrations in carbonate samples, with both being in the range of 0.50 to 3.00 ppm (Figure 4(d)).

The abundances of Ba and Eu in mudrock and chert are much higher than in carbonate rocks. In Batch 1, the concentration of Ba ranges from 431.47 to 20386.00 ppm, approximately 40 times higher than that in carbonates on average (Figure 4(a)). The concentration of Eu is in the range of 0.27 to 6.22 ppm, which is about 9 times higher than that in carbonates (Figure 4(b)). Values of Eu/Eu^* range from 1.12 to 14.17, suggesting pronounced positive Eu anomalies (Figure 4(c)). In Batch 2, the concentration of Ba and Eu ranges from 1818.70 ppm to 17316.74 ppm (Figure 4(a)) and 0.86 ppm to 3.71 ppm (Figure 4(b)), respectively. The average concentrations of Ba and Eu are 30 and 7 times higher than those in carbonates, respectively, with Eu/Eu^* values ranging from 1.08 to 11.20 (Figure 4(c)).

Table 2: Concentrations of Ba and selected REE elements of mudrock, chert, and carbonate samples in Batch 1.

Sample	Depth (m)	Petrology	Ba	Sm	Eu	Gd	Eu/Eu*
WN-1	820.60	Chert	2326.83	2.00	0.87	2.02	2.04
WN-2	820.50	Chert	1645.36	1.62	0.76	2.12	1.87
WN-3	820.30	Chert	11326.82	1.44	2.99	2.30	7.33
WN-4	819.10	Siliceous dolomite	88.55	1.03	0.20	1.00	0.93
WN-5	818.70	Chert	17987.58	1.97	4.31	2.14	9.81
WN-6	817.00	Siliceous dolomite	162.34	1.01	0.19	0.90	0.95
WN-7	810.80	Siliceous dolomite	172.38	0.88	0.17	0.88	0.91
WN-8	808.60	Siliceous dolomite	312.00	1.18	0.16	0.93	0.71
WN-9	805.00	Siliceous dolomite	326.92	2.68	0.45	2.38	0.85
WN-10	800.80	Siliceous dolomite	76.67	0.96	0.19	0.85	0.99
WN-11	797.30	Carbonaceous mudrock	11742.34	1.51	2.97	1.96	7.96
WN-12	796.00	Carbonaceous mudrock	4495.63	1.47	1.46	1.81	4.13
WN-13	794.80	Chert	2237.81	0.20	0.68	0.24	14.17
WN-14	790.60	Siliceous mudrock	8684.80	3.38	2.44	4.05	3.05
WN-15	785.50	Chert	5499.63	3.28	1.77	4.15	2.22
WN-16	780.90	Carbonaceous mudrock	3375.06	3.08	1.36	3.47	1.93
WN-17	775.60	Carbonaceous mudrock	20386.00	10.84	6.22	11.58	2.60
WN-18	775.50	Carbonaceous mudrock	1715.44	2.58	0.98	2.97	1.65
WN-19	774.70	Carbonaceous mudrock	17695.16	4.73	4.75	4.59	4.79
WN-20	772.90	Carbonaceous mudrock	5655.41	6.89	2.59	7.28	1.71
WN-21	771.00	Carbonaceous mudrock	4387.75	11.94	3.40	16.15	1.12
WN-22	770.30	Carbonaceous mudrock	7061.81	5.79	2.79	6.23	2.17
WN-23	767.30	Carbonaceous mudrock	5763.93	8.53	2.66	10.24	1.32
WN-24	765.10	Carbonaceous mudrock	3570.41	5.61	2.38	7.76	1.65
WN-25	763.30	Dolomitic mudrock	13994.26	4.22	3.83	3.57	4.64
WN-26	761.80	Carbonaceous mudrock	13725.53	3.02	3.55	2.77	5.77
WN-27	760.00	Carbonaceous mudrock	10614.46	3.87	2.81	3.42	3.63
WN-28	759.00	Carbonaceous mudrock	6452.16	3.15	1.93	3.54	2.69
WN-29	755.80	Limestone	153.80	2.50	0.38	1.69	0.86
WN-30	754.80	Chert	2420.48	2.45	1.01	2.35	1.98
WN-31	753.70	Chert	2403.92	2.44	1.06	2.23	2.15
WN-32	751.10	Carbonaceous mudrock	1871.24	3.50	1.14	4.41	1.34
WN-33	749.20	Carbonaceous mudrock	431.57	0.76	0.27	0.84	1.58
WN-34	745.50	Carbonaceous mudrock	2366.46	2.11	0.96	2.85	1.79
WN-35	742.50	Carbonaceous mudrock	3290.43	1.52	1.10	1.82	3.05
WN-36	740.60	Carbonaceous mudrock	1731.86	0.78	0.57	0.79	3.44
WN-37	739.10	Carbonaceous mudrock	961.89	1.03	0.41	1.06	1.82
WN-38	738.00	Carbonaceous mudrock	3582.52	3.61	1.57	3.98	1.94
WN-39	736.00	Carbonaceous mudrock	8760.99	4.04	2.56	4.09	2.95
WN-40	735.40	Carbonaceous mudrock	7485.79	3.55	2.33	3.65	3.03
WN-41	733.40	Carbonaceous mudrock	16004.86	7.76	5.01	8.03	2.97
WN-42	730.00	Carbonaceous mudrock	6234.39	3.59	2.16	3.83	2.73
WN-43	727.80	Carbonaceous mudrock	8528.94	4.01	2.58	4.60	2.79
WN-44	722.80	Carbonaceous mudrock	8981.91	3.93	2.85	4.26	3.26

The covariation of Sm and Gd can also be observed in mudrock and chert samples in both batches. The range becomes broader for both batches, varying from 0.78 to 16.15 ppm (Figure 4(d)).

5. Discussion

5.1. Ba-Eu Correlation. In previous studies, to evaluate the interference of Ba with Eu concentrations, correlations of

Table 3: Concentrations of REEs and Ba of mudrock and chert samples in Batch 2.

Sample	Depth (m)	Petrology	Ba	Sm	Eu	Gd	Eu/Eu*
WN2-1	794.30	Chert	17316.14	3.28	3.71	2.97	5.59
WN2-2	789.60	Siliceous mudrock	1818.70	2.07	0.85	2.41	1.76
WN2-3	787.10	Siliceous mudrock	12080.80	1.13	2.70	1.14	11.17
WN2-4	752.00	Carbonaceous mudrock	5345.38	5.16	2.33	6.63	1.83
WN2-5	747.70	Carbonaceous mudrock	6248.18	5.01	2.34	5.83	2.01
WN2-6	727.40	Carbonaceous mudrock	1024.67	3.44	0.92	4.17	1.12
WN2-7	724.90	Carbonaceous mudrock	11288.06	1.39	2.35	1.31	8.18
WN2-8	721.10	Carbonaceous mudrock	9054.77	0.85	1.97	0.81	11.20
WN2-9	716.60	Calcareous mudrock	8602.37	3.29	2.13	2.91	3.24
WN2-10	712.60	Calcareous mudrock	3462.94	1.52	1.09	1.47	3.43
WN2-11	697.80	Calcareous mudrock	1986.20	2.60	0.90	2.25	1.76
WN2-12	694.80	Calcareous mudrock	1211.51	7.52	1.52	5.86	1.08
WN2-13	693.50	Siliceous mudrock	7764.73	1.86	2.15	2.01	5.19
WN2-14	692.60	Siliceous mudrock	5303.73	2.44	1.72	2.83	3.03
WN2-15	692.50	Siliceous mudrock	4536.49	3.09	1.70	3.42	2.45
WN2-16	687.50	Carbonaceous mudrock	1895.46	2.41	0.88	2.25	1.78
WN2-17	684.00	Carbonaceous mudrock	2137.55	3.98	1.29	3.85	1.55
WN2-18	682.40	Carbonaceous mudrock	2255.65	3.24	1.00	2.83	1.55
WN2-19	681.40	Siliceous mudrock	2901.96	4.51	1.51	4.07	1.66

Ba and Eu were verified with different elemental ratios, including the relationship between Ba/Nd and Eu/Eu* ([5]; Ling et al., 2013), Eu/Eu* and Ba/Sm [20], and Ba and Eu/Eu*[25]. Among them, instead of the absolute concentration of Eu, the ratio of Eu/Eu* was the one that is frequently used to evaluate the Eu abundance. Due to intrinsic chemical properties and complex redox conditions, Sm and Gd behave differently than Eu in natural environments. Changes in their abundances may not result from the same geological event(s) that impacted the Eu speciation and its distribution in different phases. Therefore, the involvement of Sm and Gd in evaluating Ba interference with the ratio of Eu/Eu* may obscure the original Eu distribution and authentic Ba-Eu correlation. The abundances of Ba and Eu are evaluated directly in this study.

The concentrations of Ba and Eu in mudrock and chert samples in Batch 1 show a significant linear correlation, with the coefficient of determination (R^2) of the linear regression line being 0.88 (Figure 5(a)). In carbonate samples within the same batch, however, no linear Ba-Eu correlation is observed (Figure 5(b)). Concentrations of Ba and Eu in mudrock and chert samples in Batch 2 have also shown linearity between them, with an R^2 of 0.86 (Figure 5(c)). By combining data from both Batch 1 and Batch 2, a linear Ba-Eu correlation with an overall R^2 of 0.85 suggests a consistent relation between Ba and Eu in mudrock and chert samples (Figure 5(d)), with the Ba/Eu ratios ranging from 797.32 to 4806.16.

The abundance of Eu (i.e., Eu_T), reported as the result collected by ICP-MS, has two potential sources: the authentic Eu content in samples (Eu_A) and the signal error caused by Ba interference (Eu_F). The value of Eu_A is the direct result of involved geological processes, while Eu_F is linearly correlated with the Ba concentration. If Eu_F is much higher than Eu_A, a linear Ba-Eu_T correlation most likely indicates major interferences from Ba. This is how linear Ba-Eu_T correlations were interpreted in previous studies ([5, 20, 25]; Ling et al., 2013). However, if Ba and Eu_A are enriched by the same geological processes and the abundance of Eu_A is dominant in the total Eu, a Ba-Eu linear correlation is a genuine record of geochemical processes involving both elements. Both possibilities are discussed in the following sections to unravel the cause of linear Ba-Eu_T correlations in this study.

5.2. Evaluation of Analytical Interferences. The interference of Ba in the determination of Eu was a systematic error caused by the overlap of peaks from Ba oxide and hydroxide species with Eu isotopes during ICP-MS analysis [21]. Due to the difference in system errors of individual instruments and internal standards used, the ratio of the concentration of Ba over Eu_F could vary significantly between different instruments. For example, the Ba/Eu_F ratios of 1000 : 0.22 and 1000 : 0.10 from ICP-MS analyses were reported by Dulski [21] and Smirnova et al. [24], respectively. Despite this discrepancy, for the same instrument, the Ba/Eu_F ratio is believed to be constant under similar working conditions [21].

As reported above in "Introduction," to validate the extent of Ba interference on Eu, the most effective method is to determine the yield of Eu caused by single-element solutions of Ba oxide or hydroxide with varying concentrations [21, 24]. Such experiment has been conducted on a Finnigan Element XR ICP-MS in the same laboratory, with identical pretreatment procedures and similar analytical

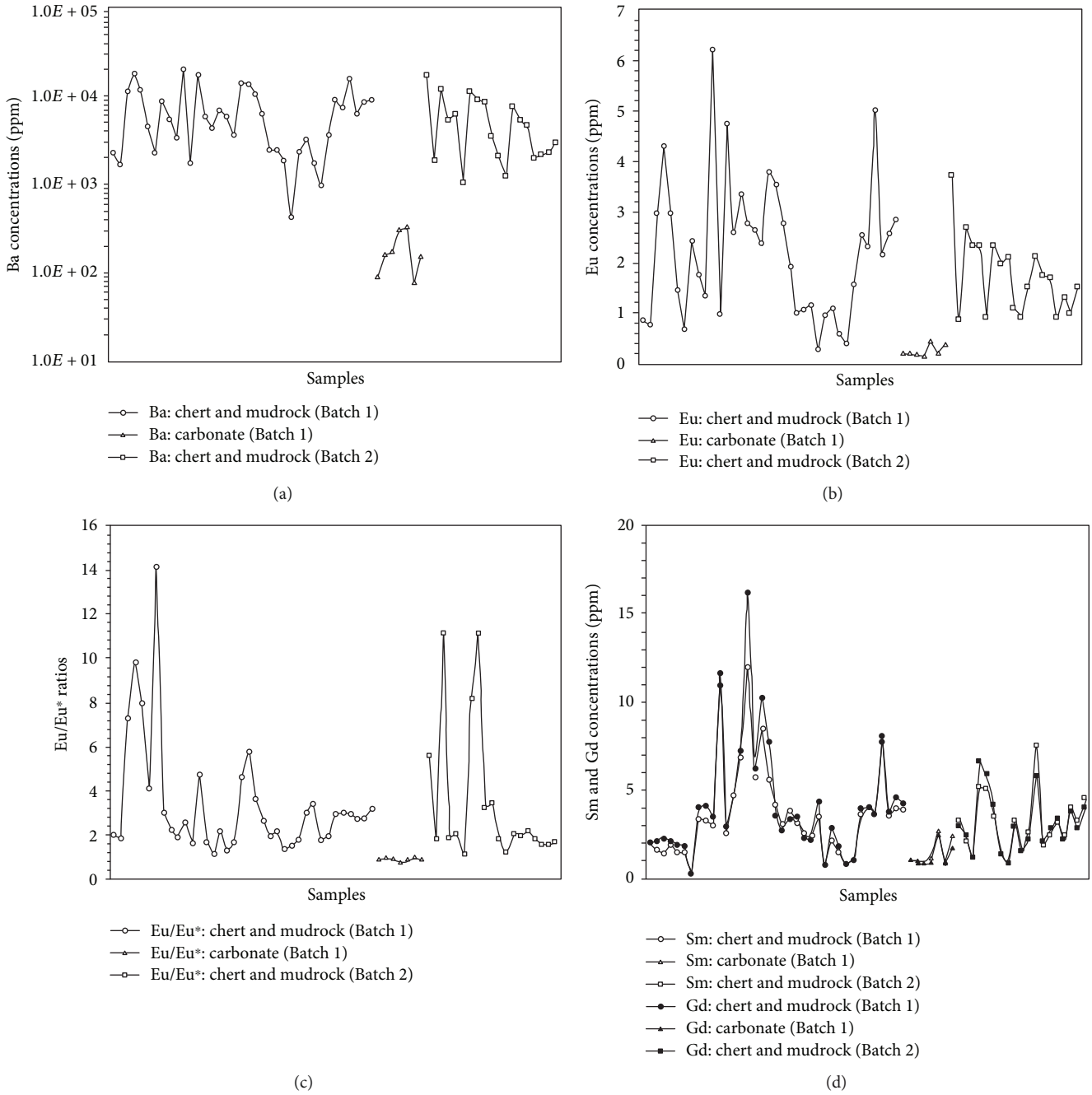

Figure 4: The plots showing values of (a) Ba concentrations, (b) Eu concentrations, (c) Eu/Eu* ratios, and (d) Sm and Gd concentrations in chert and mudrock samples for Batch 1, carbonate samples for Batch 1, and chert and mudrock samples for Batch 2.

conditions to the Finnigan Element II ICP-MS used in this study [33]. The results revealed a Ba/Eu_F ratio of 400000 : 1 to 1400000 : 1 for the low-resolution (300) mode analysis and much higher Ba/Eu_F ratios for the mid-resolution (4000) and high-resolution (10000) mode analyses. In this case, the Ba/Eu_F ratio was supposed to be at least 100 times higher than the Ba/Eu_A ratio of analyzed samples in this study, demonstrating that the extent of Ba interference on Eu determination was likely minimal.

In addition, previously published data of Ba and Eu_T concentrations obtained from the same instrument under similar working conditions are also collected to evaluate the Ba/Eu_F ratio. In a study of black shale in the Niutitang Formation (lower Cambrian) in South China, the concentrations of Ba and Eu_T were reported to be in the ranges of 659 to 13686 ppm and 0.33 to 3.97 ppm, respectively [15] (Figure 6(a)). The Ba/Eu_T ratio was calculated to be varied from 391.54 to 8146.43. Both the Ba and Eu concentrations in black shale, along with their ratios (Ba/Eu_T), are in a similar range as in samples of this study (Tables 2 and 3). However, no linear correlation between Ba and Eu_T can be extracted in spite of a weak covariation

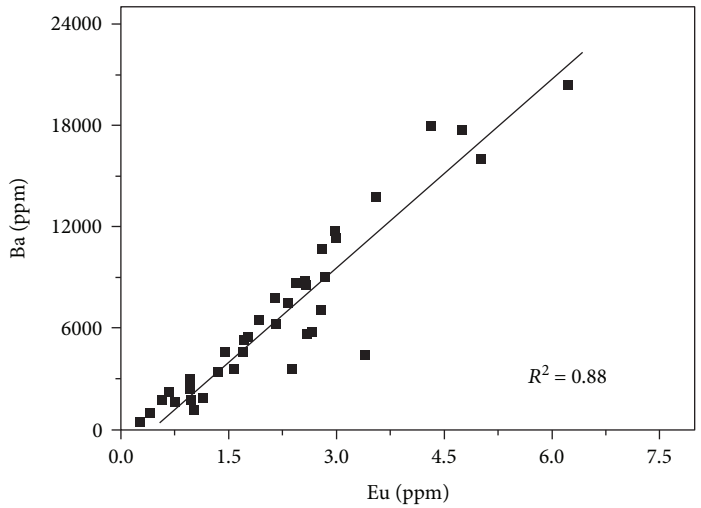

(a)

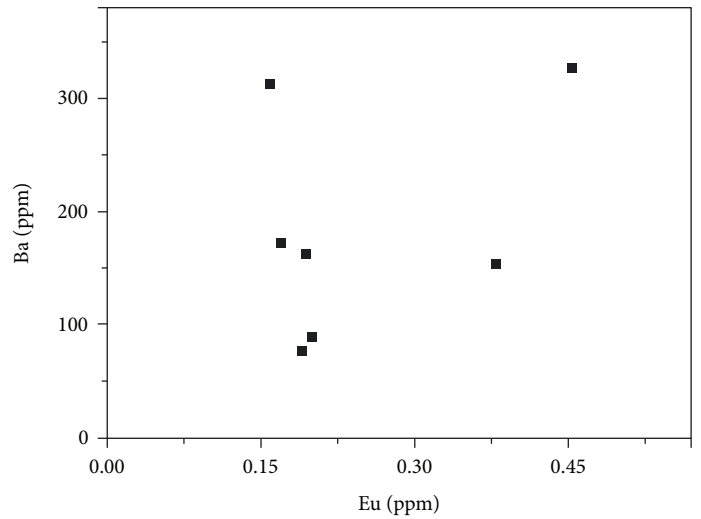

(b)

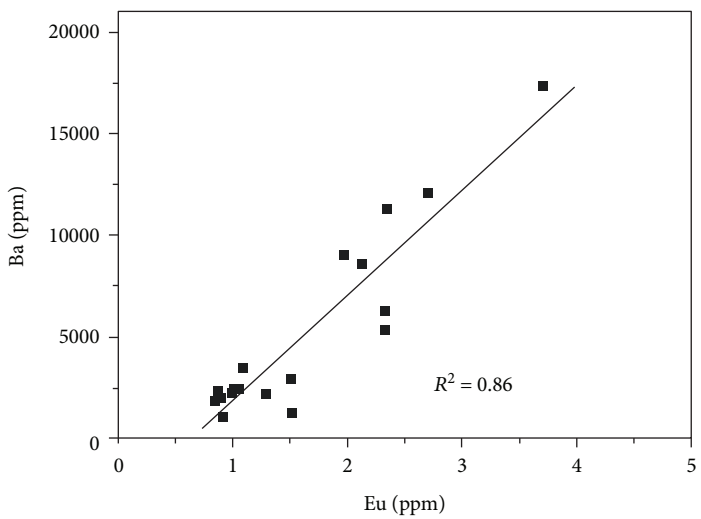

(c)

Figure 5: Continued.

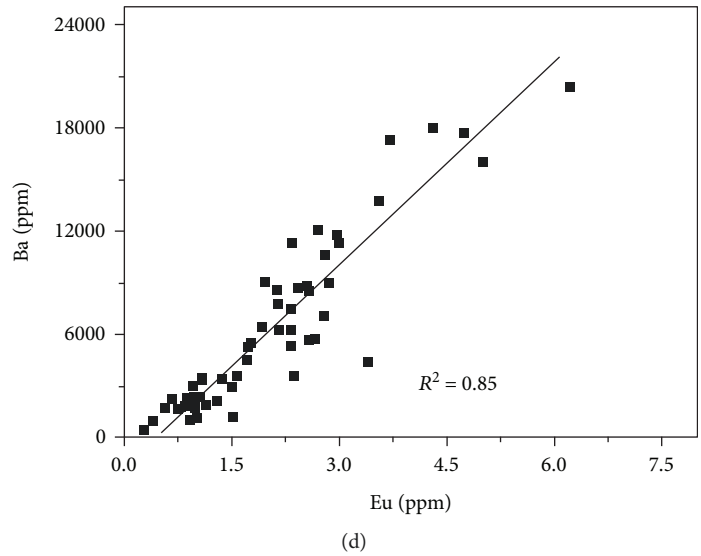

Figure 5: The plots showing Ba and Eu contents in samples of this study. (a) Concentrations of Ba and Eu in mudrock and chert for Batch 1. A linear correlation with an R^2 of 0.88 is observed. (b) Concentrations of Ba and Eu in carbonate rocks for Batch 1. No linear correlation is observed. (c) Concentrations of Ba and Eu in mudrock and chert for Batch 2. A linear correlation with an R^2 of 0.86 is observed. (d) Concentrations of Ba and Eu in mudrock and chert for Batch 1 and Batch 2. A linear Ba-Eu correlation with an R^2 of 0.85 is observed.

trend, suggesting that Eu_F is not a major component of the reported Eu_T values.

Another set of data comparable to this study was reported on phosphate nodules of the Mufushan Formation, which is also in the period of lower Cambrian in South China [20]. The Ba and Eu_T concentrations are in a narrower range than other reported data, from 817 to 6144 ppm and 0.05 to 11.42 ppm, respectively (Figure 6(b)). The Ba/Eu_T ratio varies significantly from 95.53 to 59040.00. There is no linear correlation between Ba and Eu_T (Figure 6(b)). Therefore, considering the similar range of Ba concentrations and Ba/Eu_T ratios obtained in this study, systematic analytical errors can be excluded as a main factor attributing to the significant linear correlation between Ba and Eu.

Furthermore, the concentrations of Sm and Eu from most samples in this study have also shown a positive correlation (Figure 7(a)). A similar relationship can be observed between Eu and Gd as well (Figure 7(b)). Unlike Eu, the interference of Ba on Sm and Gd is believed to be negligible because of differences in mass over charge ratio [21]. Therefore, the linear Ba-Eu correlation, coupled with Eu-Sm and Eu-Gd linearities, suggests the presence of an intrinsic relationship between Ba and Eu which is mainly caused by geological processes. The positive Eu-Sm and Eu-Gd correlations in this study may result from the impact of the geological processes and the original elemental feature of the sediments.

5.3. Evidence of Ba-Eu Coexistence. Europium is commonly enriched in plagioclase as a result of substitution into the calcium site. Similar to Ca^{2+}, Ba^{2+} can also be substituted by Eu^{2+} due to the same electronic charge and similar cation radius [34–36]. Therefore, Eu may be enriched in minerals or geological fluids that have high abundances of Ba. A linear Ba-Eu correlation can be present as a result of their substitutional relationship, particularly when Ba^{2+} is the dominant cation in minerals (or geological fluids) as shown above (Figures 4(a), 4(c) and 4(d)).

The linear relationship between Ba and Eu suggests that the majority of Ba and Eu in this set of rock formations are closely related during geological processes. The BSE observation and elemental analysis by EMPA provide additional evidence showing the highly concentrated areas of Ba in the samples. The Ba-rich minerals, hyalophane in particular, are pervasive in the rock sequence and present in the matrix of all the samples analyzed by EMPA (Figure 2). Hyalophane is believed to be formed in limited geological environments, and its origin is mostly from hydrothermal fluids (McSwiggen et al., 1994; Moro et al., 2001).

In the rock matrix, hyalophane mainly occurs as rims of clastic K-feldspars (Figure 3(c)). Both hyalophane and cymrite are also present in intergranular pores (Figure 3(a)). The hydrothermal veins containing hyalophane are common textures, shown penetrating into the matrix (Figures 3(b) and 3(c)). Overall, the occurrence of such Ba-rich minerals suggests that they were formed by infiltration of late-stage hydrothermal fluids into the rocks. Hyalophane of hydrothermal origin with similar occurrences (e.g., hyalophane rims around K-feldspar) was also found in black shale in the Devonian period from the Selwyn Basin, Canada [37].

In this study, both barium and europium elements are concentrated by late-stage hydrothermal fluids passing through surrounding sedimentary sequences. They were then accumulated in hyalophane and cymrite during diagenesis. This scenario agrees well with the consistently high concentration of Ba in the chert and mudrock samples analyzed, with an average value of 6431.04 ppm (Tables 2 and 3). It is also confirmed by the fact that, as hyalophane and cymrite

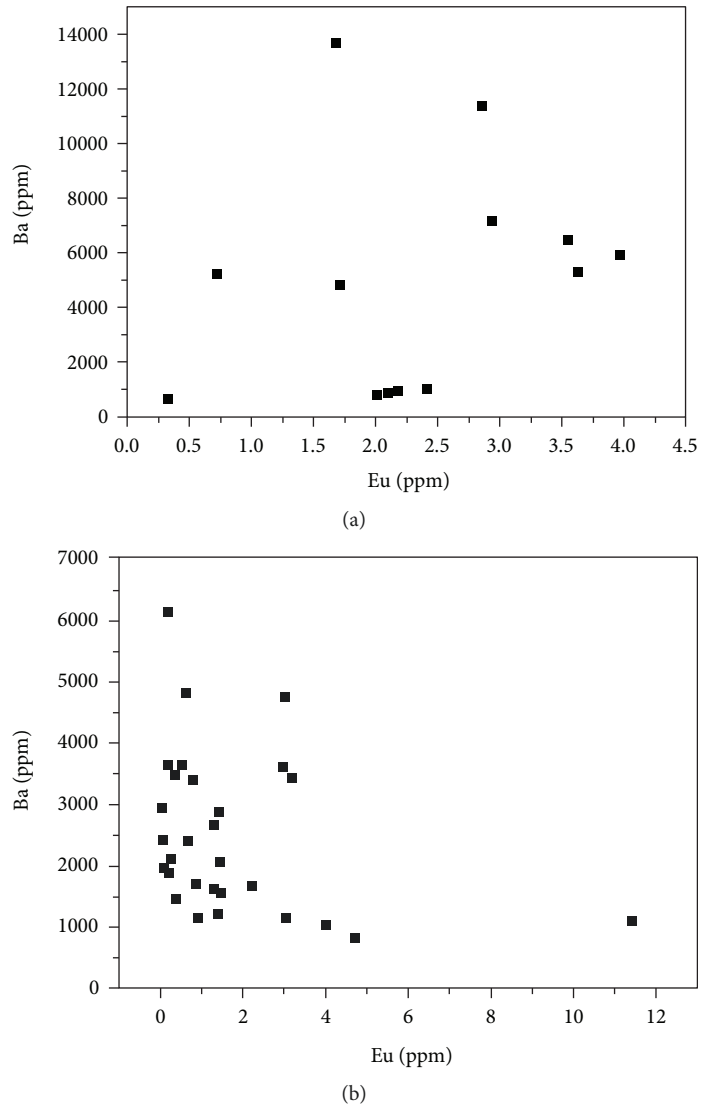

Figure 6: The Ba and Eu data reported in previous studies using the same instrument. (a) Ba and Eu from shale in the Niutitang Formation, South China [15]. The Ba/Eu ratio was varied from 391.54 to 8146.43. (b) Ba and Eu from phosphate nodules in the Mufushan Formation [20]. The Ba/Eu ratio ranges from 95.53 to 59040.00.

are not included in the trace element and rare earth element analyses of carbonate rocks because they are insoluble in HAC, lower Ba concentrations and nonlinear Ba-Eu correlation are obtained (Figures 4(a) and 5(b)).

Enrichment of Eu has been reported in modern deep-sea hydrothermal systems [7–9] and in massive deposits of submarine hydrothermal exhalative origin [10–12]. High abundances of both Ba and Eu in hydrothermal fluids are present in a variety of hydrothermal environments [7, 38–40].

Wang et al. [25] investigated the occurrences and textures of chert on the marginal zone of the Yangtze platform in the western Hunan area, during the Ediacaran-Cambrian transition. Four lithotypes of chert are identified in the study, including mounded, vein, brecciated, and bedded chert. Further geochemical investigations have shown prevalent positive Eu anomalies in chert and homogenization temperature of fluid inclusions in the range of 120-180°C. Consequently, the chert was suggested to be formed by hydrothermal fluids. The variation of occurrences and textures was considered to be a reflection of different formation conditions. The mounded chert was formed at or near the vent fields, while the formation of brecciated chert occurred in large-scale fracture systems. The chert in veins was precipitated from silica-rich hydrothermal fluids ascending along fractures, and the bedded chert was formed in a quiet water environment away from vent fields. This wide range of occurrences of hydrothermal chert was ascribed to the extensional tectonism in the Yangtze Block during the Ediacaran-Cambrian transition [25, 41].

Although the positive Eu anomaly was observed in most chert samples, barite was only found in mounded and brecciated chert. Only in those two lithotypes of chert can a prominent linear Ba-Eu correlation be extracted (Figure 8(a)). No

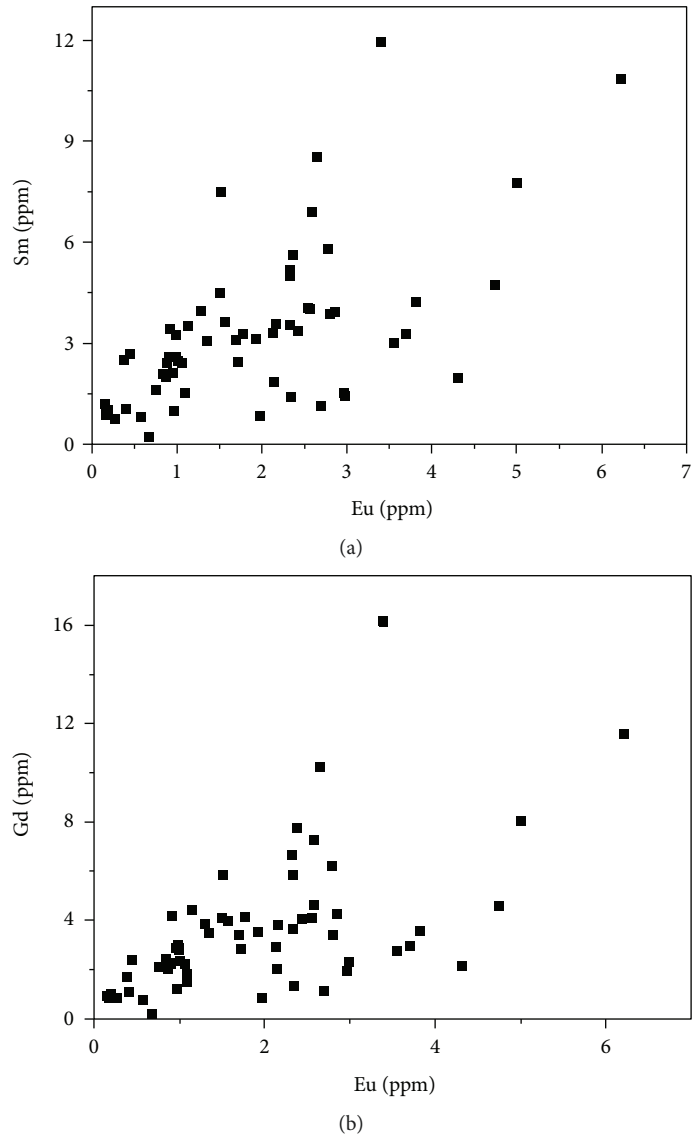

Figure 7: The plots showing the relationship between trace elements in this study. (a) Eu and Sm. (b) Eu and Gd. The Eu-Sm and Eu-Gd correlations can be observed in (a) and (b), respectively.

significant Ba-Eu correlation can be recognized in the other two types of chert (Figure 8(b)), although the concentration of Ba and the Ba/Eu ratio of bedded chert are in a similar range as those of mounded and brecciated chert.

The results above provide another line of evidence supporting that the distinct Ba-Eu correlations in different lithotypes of chert are caused by the source of elements and environmental conditions. In areas close to vent fields or having large-scale fracture systems, where the mounded and brecciated chert were formed, chemical components in hydrothermal fluids can be preserved. However, bedded chert was suggested to form far away from vent fields and in a quiet water environment, where the original correlation between Ba and Eu contents within hydrothermal fluids could be erased by secondary processes. Therefore, we suggest that the linear Ba-Eu correlation in mounded and brecciated chert most likely is being caused by significant contribution from Ba-rich hydrothermal fluids.

6. Conclusions

Trace elemental analysis of the lower Cambrian Hetang Formation in Anhui Province has shown a linear relationship between Ba and Eu contents in mudrock and chert formations. Combined with petrological and mineralogical observation, significant contribution of Ba and Eu from Ba-rich hydrothermal fluids is proposed to account for that correlation. Positive Eu anomaly in the rocks is suggested to be an effective record of the influence of hydrothermal activities.

The ratio of Ba/Eu provides important information for evaluating the interference of Ba on determination of Eu concentrations during analysis. Relatively low Ba/Eu ratios and significant linear Ba-Eu correlations may suggest that Ba and Eu were originated from the same hydrothermal source. In addition, petrological and mineralogical investigations are essential in identifying the occurrences of Ba and Eu in rocks and facilitating understanding of Ba-Eu correlations.

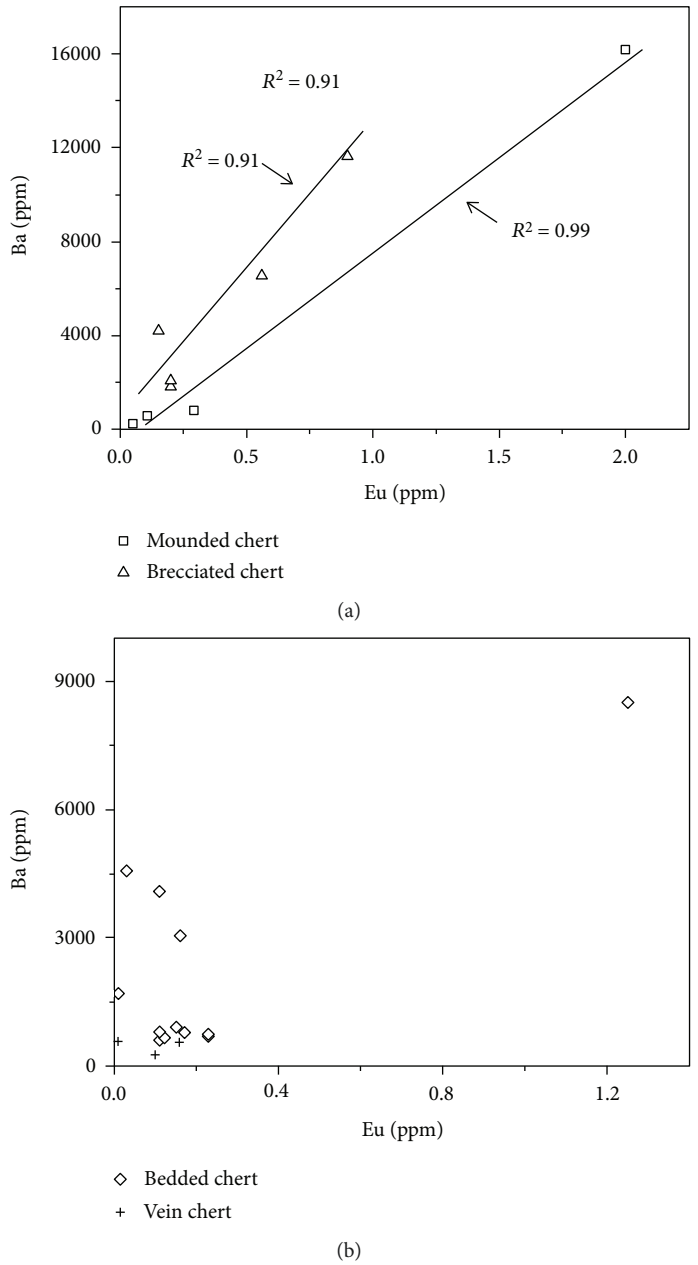

Figure 8: Correlations of Ba and Eu contents in (a) mounded and brecciated chert and (b) vein and bedded chert in the work of Wang et al. [25]. Linear correlations with R^2 of 0.99 and 0.91 are observed in mounded and brecciated chert, respectively.

At the western boundary of the Yangtze platform, pronounced linear Ba-Eu correlations were also present in barite-bearing chert (mounded and brecciated chert) formed by Ba-rich hydrothermal fluids. We suggest that such linear Ba-Eu correlations may be common in geological environments, which is ultimately constrained by the availability of both elements in rock sequences and the timing of hydrothermal activities.

Data Availability

The trace and rare earth element data used to support the findings of this study are included within the article.

Conflicts of Interest

The authors declare that they have no conflicts of interest.

Acknowledgments

This study was financially supported by the National Key Research and Development Program (Grant no. 2017YFC0603101), National Natural Science Foundation of China (Grant nos. 41802026, 41830425, 41890845, and 41621003), China Postdoctoral Science Foundation (Grant no. 2018M633553), and 111 Project (D17013). Research support to QF from the NSF CAREER Program under award OCE-

1652481 and the American Chemical Society Petroleum Research Fund 54474-DNI2 is also acknowledged. Special thanks are due to Dr. Wenlan Zhang and Qian Liu for their help with analytical work.

References

[1] J. R. Haas, E. L. Shock, and D. C. Sassani, "Rare earth elements in hydrothermal systems: estimates of standard partial molal thermodynamic properties of aqueous complexes of the rare earth elements at high pressures and temperatures," *Geochimica et Cosmochimica Acta*, vol. 59, no. 21, pp. 4329–4350, 1995.

[2] Y. H. Jiang, Z. Liu, R. Y. Jia, S. Y. Liao, Q. Zhou, and P. Zhao, "Miocene potassic granite–syenite association in western Tibetan Plateau: implications for shoshonitic and high Ba–Sr granite genesis," *Lithos*, vol. 134-135, pp. 146–162, 2012.

[3] H. J. W. de Baar, M. P. Bacon, P. G. Brewer, and K. W. Bruland, "Rare earth elements in the Pacific and Atlantic Oceans," *Geochimica et Cosmochimica Acta*, vol. 49, no. 9, pp. 1943–1959, 1985.

[4] P. Henderson, Ed., *Rare Earth Element Geochemistry*, Elsevier, 1984.

[5] G. Shields and P. Stille, "Diagenetic constraints on the use of cerium anomalies as palaeoseawater redox proxies: an isotopic and REE study of Cambrian phosphorites," *Chemical Geology*, vol. 175, no. 1-2, pp. 29–48, 2001.

[6] J. J. Álvaro, G. A. Shields-Zhou, P. Ahlberg, S. Jensen, and T. Palacios, "Ediacaran–Cambrian phosphorites from the western margins of Gondwana and Baltica," *Sedimentology*, vol. 63, no. 2, pp. 350–377, 2016.

[7] E. Douville, P. Bienvenu, J. L. Charlou et al., "Yttrium and rare earth elements in fluids from various deep-sea hydrothermal systems," *Geochimica et Cosmochimica Acta*, vol. 63, no. 5, pp. 627–643, 1999.

[8] A. Michard, F. Albarède, G. Michard, J. F. Minster, and J. L. Charlou, "Rare-earth elements and uranium in high-temperature solutions from East Pacific Rise hydrothermal vent field (13 °N)," *Nature*, vol. 303, no. 5920, pp. 795–797, 1983.

[9] R. M. Owen and A. M. Olivarez, "Geochemistry of rare earth elements in pacific hydrothermal sediments," *Marine Chemistry*, vol. 25, no. 2, pp. 183–196, 1988.

[10] T. J. Barrett, I. Jarvis, and K. E. Jarvis, "Rare earth element geochemistry of massive sulfides-sulfates and gossans on the Southern Explorer Ridge," *Geology*, vol. 18, no. 7, pp. 583–586, 1990.

[11] J. L. Graf, "Rare earth elements as hydrothermal tracers during the formation of massive sulfide deposits in volcanic rocks," *Economic Geology*, vol. 72, no. 4, pp. 527–548, 1977.

[12] J. M. Peter and W. D. Goodfellow, "Mineralogy, bulk and rare earth element geochemistry of massive sulphide-associated hydrothermal sediments of the Brunswick Horizon, Bathurst Mining Camp, New Brunswick," *Canadian Journal of Earth Sciences*, vol. 33, no. 2, pp. 252–283, 1996.

[13] C. S. Eker, F. Sipahi, and A. Kaygusuz, "Trace and rare earth elements as indicators of provenance and depositional environments of Lias cherts in Gumushane, NE Turkey," *Chemie der Erde*, vol. 72, no. 2, pp. 167–177, 2012.

[14] S. Y. Jiang, J. M. Yu, and J. J. Lu, "Trace and rare-earth element geochemistry in tourmaline and cassiterite from the Yunlong tin deposit, Yunnan, China: implication for migmatitic-hydrothermal fluid evolution and ore genesis," *Chemical Geology*, vol. 209, no. 3-4, pp. 193–213, 2004.

[15] S. Y. Jiang, Y. Q. Chen, H. F. Ling, J. H. Yang, H. Z. Feng, and P. Ni, "Trace- and rare-earth element geochemistry and Pb–Pb dating of black shales and intercalated Ni–Mo–PGE–Au sulfide ores in lower Cambrian strata, Yangtze platform, South China," *Mineralium Deposita*, vol. 41, no. 5, pp. 453–467, 2006.

[16] J. Pan, D. Ma, and S. Cao, "Trace element geochemistry of the lower Cambrian black rock series from northwestern Hunan, South China," *Progress in Natural Science*, vol. 14, no. 1, pp. 64–70, 2004.

[17] M. Steiner, E. Wallis, B. D. Erdtmann, Y. Zhao, and R. Yang, "Submarine-hydrothermal exhalative ore layers in black shales from South China and associated fossils — insights into a lower Cambrian facies and bio-evolution," *Palaeogeography, Palaeoclimatology, Palaeoecology*, vol. 169, no. 3-4, pp. 165–191, 2001.

[18] K. D. Zhao and S. Y. Jiang, "Rare earth element and yttrium analyses of sulfides from the Dachang Sn-polymetallic ore field, Guangxi province, China: implication for ore genesis," *Geochemical Journal*, vol. 41, no. 2, pp. 121–134, 2007.

[19] B. Zhu, S. Y. Jiang, J. H. Yang, D. Pi, H. F. Ling, and Y. Q. Chen, "Rare earth element and Sr-Nd isotope geochemistry of phosphate nodules from the lower Cambrian Niutitang Formation, NW Hunan Province, South China," *Palaeogeography Palaeoclimatology Palaeoecology*, vol. 398, no. 3, pp. 132–143, 2014.

[20] S. Y. Jiang, H. X. Zhao, Y. Q. Chen, T. Yang, J. H. Yang, and H. F. Ling, "Trace and rare earth element geochemistry of phosphate nodules from the lower Cambrian black shale sequence in the Mufu Mountain of Nanjing, Jiangsu province, China," *Chemical Geology*, vol. 244, no. 3-4, pp. 584–604, 2007.

[21] P. Dulski, "Interferences of oxide, hydroxide and chloride analyte species in the determination of rare earth elements in geological samples by inductively coupled plasma-mass spectrometry," *Fresenius Journal of Analytical Chemistry*, vol. 350, no. 4-5, pp. 194–203, 1994.

[22] S. Wu, X. Zeng, X. Dai, Y. Hu, G. Li, and C. Zheng, "Accurate determination of ultra-trace impurities, including europium, in ultra-pure barium carbonate materials through inductively coupled plasma–tandem mass spectrometry," *Spectrochimica Acta Part B: Atomic Spectroscopy*, vol. 123, pp. 129–133, 2016.

[23] X. Yan, S. Dai, I. T. Graham, X. He, K. Shan, and X. Liu, "Determination of Eu concentrations in coal, fly ash and sedimentary rocks using a cation exchange resin and inductively coupled plasma mass spectrometry (ICP-MS)," *International Journal of Coal Geology*, vol. 191, pp. 152–156, 2018.

[24] E. V. Smirnova, I. N. Fedorova, G. P. Sandimirova, L. L. Petrov, N. G. Balbekina, and V. I. Lozhkin, "Determination of rare earth elements in black shales by inductively coupled plasma mass spectrometry," *Spectrochimica Acta Part B: Atomic Spectroscopy*, vol. 58, no. 2, pp. 329–340, 2003.

[25] J. Wang, D. Chen, D. Wang, D. Yan, X. Zhou, and Q. Wang, "Petrology and geochemistry of chert on the marginal zone of Yangtze platform, western Hunan, South China, during the Ediacaran-Cambrian transition," *Sedimentology*, vol. 59, no. 3, pp. 809–829, 2012.

[26] S. Han, K. Hu, J. Cao, J. Pan, F. Xia, and W. Wu, "Origin of early Cambrian black-shale-hosted barite deposits in South China: mineralogical and geochemical studies," *Journal of Asian Earth Sciences*, vol. 106, pp. 79–94, 2015.

[27] H. B. Long, J. C. Long, Y. R. Zhong, S. J. Zhuang, and T. Liu, "Discovery of hyalophane from the vanadium deposit in the black rock series at Zhangcun-Zhengfang: evidence for hydrothermal sedimentary origin," *Chinese Science Bulletin*, vol. 39, pp. 636–638, 1994.

[28] F. Xia, D. S. Ma, J. Y. Pan et al., "EMP study of early Cambrian barite deposits in eastern Guizhou, China," *Acta Mineralogica Sinica*, vol. 25, no. 3, pp. 289–294, 2005.

[29] D. Chen, J. Wang, H. Qing, D. Yan, and R. Li, "Hydrothermal venting activities in the early Cambrian, South China: petrological, geochronological, and stable isotopic constraints," *Chemical Geology*, vol. 258, no. 3-4, pp. 168–181, 2009.

[30] J. Wang and Z. X. Li, "History of Neoproterozoic rift basins in South China: implications for Rodinia break-up," *Precambrian Research*, vol. 122, no. 1-4, pp. 141–158, 2003.

[31] J. F. Gao, J. J. Lu, M. Y. Lai, Y. P. Lin, and W. Pu, "Analysis of trace elements in rock samples using HR-ICPMS," *Journal of Nanjing University (Natural Sciences)*, vol. 39, no. 6, pp. 844–850, 2003.

[32] S. R. Taylor and S. M. McLennan, *The Continental Crust: Its Composition and Evolution*, Blackwell, London, UK, 1985.

[33] B. Zhu, Q. Liu, and T. Yang, "Matrix effect on barium oxide and hydroxide formation during ICP-MS measurement and Its implication for Eu correction," *Geological Journal of China Universities*, vol. 22, no. 3, pp. 467–473, 2016.

[34] F. Guichard, T. M. Church, M. Treuil, and H. Jaffrezic, "Rare earths in barites: distribution and effects on aqueous partitioning," *Geochimica et Cosmochimica Acta*, vol. 43, no. 7, pp. 983–997, 1979.

[35] A. Mazumdar, D. M. Banerjee, M. Schidlowski, and V. Balaram, "Rare-earth elements and stable isotope geochemistry of early Cambrian chert-phosphorite assemblages from the lower Tal Formation of the Krol Belt (Lesser Himalaya, India)," *Chemical Geology*, vol. 156, no. 1-4, pp. 275–297, 1999.

[36] R. D. Shannon, "Revised effective ionic radii and systematic studies of interatomic distances in halides and chalcogenides," *Acta Crystallographica Section A*, vol. 32, no. 5, pp. 751–767, 1976.

[37] B. Orberger, J. P. Gallien, D. L. Pinti et al., "Nitrogen and carbon partitioning in diagenetic and hydrothermal minerals from Paleozoic black shales, (Selwyn Basin, Yukon Territories, Canada)," *Chemical Geology*, vol. 218, no. 3-4, pp. 249–264, 2005.

[38] K. Bostroem, H. Rydell, and O. Joensuu, "Langban; an exhalative sedimentary deposit?," *Economic Geology*, vol. 74, no. 5, pp. 1002–1011, 1979.

[39] C. Cai, K. Li, H. Li, and B. Zhang, "Evidence for cross formational hot brine flow from integrated $^{87}Sr/^{86}Sr$, REE and fluid inclusions of the Ordovician veins in Central Tarim, China," *Applied Geochemistry*, vol. 23, no. 8, pp. 2226–2235, 2008.

[40] R. H. James, D. E. Allen, and W. E. Seyfried Jr., "An experimental study of alteration of oceanic crust and terrigenous sediments at moderate temperatures (51 to 350°C): insights as to chemical processes in near-shore ridge-flank hydrothermal systems," *Geochimica et Cosmochimica Acta*, vol. 67, no. 4, pp. 681–691, 2003.

[41] H. Fan, H. Wen, X. Zhu, R. Hu, and S. Tian, "Hydrothermal activity during Ediacaran–Cambrian transition: silicon isotopic evidence," *Precambrian Research*, vol. 224, no. 224, pp. 23–35, 2013.